Dalton Transactions

ROYAL SOCIETY OF CHEMISTRY

PAPER

View Article Online
View Journal | View Issue

Cite this: *Dalton Trans.*, 2022, **51**, 10898

A low-temperature thermal ALD process for nickel utilizing dichlorobis(triethylphosphine)nickel(II) and 1,4-bis(trimethylgermyl)-1,4-dihydropyrazine†

Anton Vihervaara, [a] Timo Hatanpää, [a] Kenichiro Mizohata, [b] Mykhailo Chundak, [a] Georgi Popov [a] and Mikko Ritala *[a]

Received 29th April 2022,
Accepted 24th June 2022

DOI: 10.1039/d2dt01347a

rsc.li/dalton

In this work, we developed a new ALD process for nickel metal from dichlorobis(triethylphosphine)nickel (II) ($NiCl_2(PEt_3)_2$) and 1,4-bis(trimethylgermyl)-1,4-dihydropyrazine ($(Me_3Ge)_2DHP$). A series of phosphine adducts of nickel and cobalt halides were synthesized and characterized for their volatility and thermal stability. Also $(Me_3Ge)_2DHP$ is a novel reducing agent in ALD. Smooth nickel films were deposited on different substrate materials at 110 °C, which is the lowest deposition temperature for Ni metal found in the literature. The growth rate is 0.2 Å per cycle when the film is not continuous and decreases to 0.1 Å per cycle after the film becomes pinhole-free. Besides a small amount (7 at%) of carbidic carbon, the films have only small amounts of impurities. Most notably, the chlorine content is below 0.2 at%, indicating efficient reduction. Furthermore, we think that $(Me_3Ge)_2DHP$ can open new avenues for the ALD of other metals at low temperatures.

Introduction

Nickel thin films may be used in different applications ranging from microelectronics to protective coatings[1] and catalysis.[2,3] Ni is one of the candidates for replacing copper in future interconnects in integrated circuits (IC) as it has low resistivity and a low electron mean free path, which causes the resistivity to become lower than that of copper when the interconnect dimensions are made small enough.[4] For example, cobalt was calculated to surpass copper in conductivity when the line width goes below 10 nm and nickel has similar bulk resistivity with even a lower electron mean free path than cobalt.[5] The Ni films deposited on silicon can be converted to NiSi, a low-resistivity contact material, by heating the films. Fully silicided Ni gates can be used in complementary metal oxide semiconductors.[6] Due to its ferromagnetic properties, nickel is essential for the development of magnetic memory. Spin-transfer torque magnetoresisitive random-access memory (STT-MRAM) has been considered as universal memory that may revolutionize the whole microelectronics industry someday.[7]

For the majority of future applications, it is essential to have high-quality thin films deposited uniformly over large areas and on complex 3D structures. The best method to meet these requirements is atomic layer deposition (ALD). ALD relies on saturated alternate surface reactions that provide conformal and uniform film growth across the substrate. Usually the surface reactions are activated thermally, but also plasma activation is used increasingly. About half of the reported nickel ALD processes are thermal processes and the other half are plasma processes. While plasma processes have advantages like low deposition temperature, thermal ALD is generally preferred as plasma may damage the underlying substrate material or compromise the conformality of the film. Thermal ALD is also easier to use in industry as the reactor design is simpler and batch processing is possible. However, the development of thermal ALD processes for Ni has been hindered by the lack of suitable precursors and precursor combinations. The lack of efficient reducing agents is especially apparent and many of the found reducing agents work only with specific metal precursors. A low deposition temperature is also desirable, as it generally results in smoother films, less agglomeration and thus continuous films at lower thickness.

Metallic nickel has been successfully deposited *via* ALD from a selection of nickel precursors and reducing agents. Molecular hydrogen has been used to deposit nickel films with bis(acetylacetonato)nickel(II) ($Ni(acac)_2$) at 250 °C but this process worked only on metal substrates and no properties of the films were provided.[8] Bis(*N*,*N*′-diisopropylacetamidinato) nickel(II) ($Ni(iPrAMD)_2$) was also used with H_2 at 250 °C and

[a]*Department of Chemistry, University of Helsinki, P. O. Box 55, FI-00014 Helsinki, Finland. E-mail: mikko.ritala@helsinki.fi*
[b]*Department of Physics, University of Helsinki, P. O. Box 43, FI-00014 Helsinki, Finland*

† Electronic supplementary information (ESI) available. See DOI: https://doi.org/10.1039/d2dt01347a

this process worked on both metal and non-metal substrates. The process had a growth rate of only 0.04 Å per cycle however.[9] Likewise, the bis(dimethylamino-2-methyl-2-butoxo) nickel(II) ($Ni(dmamb)_2$) + H_2 process worked at 200–250 °C on a silicon surface, but these Ni films had up to 25 at% of carbon, indicating possible precursor decomposition.[10] Also, ammonia was used with $Ni(dmamb)_2$ and high-quality Ni films were obtained (resistivity of 25 μΩ cm), but the required deposition temperature was quite high, 300 °C.[11] Using hydrazine with $Ni(acac)_2$(tmeda) (tmeda = *N*,*N*,*N*′,*N*′-tetramethylethylenediamine) at 240–280 °C resulted in high-quality Ni films (95 at% Ni and resistivity of 18 μΩ cm) with a high growth rate of 2.1 Å per cycle.[12] $Ni(acac)_2(py)_2$ (py = pyridine) also reacted with hydrazine but this combination had a lower growth rate of 0.8 Å per cycle. In one study, hydrazine was combined with $Ni(dmap)_2$ and formic acid in a three-step process which did result in a deposition of metallic nickel.[13] Another three-step process for the ALD of Ni utilized bis(1,4-di-*tert*-butyl-1,3-diazadienyl)nickel(II) ($Ni(^tBu_2DAD)_2$), formic acid and 1,4-bis(trimethylsilyl)-1,4-dihydropyrazine ($(Me_3Si)_2DHP$) at 180 °C.[14] The films deposited with this process were 94 at% nickel.

tert-Butylamine ($^tBuNH_2$) combined with $Ni(^tBu_2DAD)_2$ at 160–220 °C resulted in high-quality Ni films (>97 at% Ni and a resistivity of 22 μΩ cm), but this process worked only on metal surfaces. The growth rate was 0.6 Å per cycle.[15] Similarly, boranedimethylamine (BH_3NHMe_2) combined with bis(1-(*tert*-butylimino)-2,3-dimethylbutan-2-olate)nickel(II) ($Ni(tbidmb)_2$) at 180 °C resulted in film growth only on the Ru substrates.[16] Finally, high-purity (95 at% Ni and a resistivity of 27 μΩ cm) Ni films were obtained using $Ni(acac)_2$ and methanol at 250–300 °C, although the growth rate was fairly low (0.07 Å per cycle).[17]

Out of the reported thermal Ni ALD processes, some are applicable only on metallic substrates, which is beneficial for area-selective deposition but otherwise a limitation, and some others require relatively high deposition temperatures. The only low-temperature processes (<200 °C) are those utilizing Ni $(tbidmb)_2$ and $BH_3(NHMe_2)$ (180 °C),[16] and $Ni(^{tBu}dad)_2$ and $^tBuNH_2$ (160–220 °C).[15] However, these processes too deposit films only on metallic substrates. It also seems that many reducing agents work only with certain metal precursors and therefore do not act as general reducing agents.

Other reducing agents that can be used in ALD include metal hydrides. Tributyltin hydride and tributylgermanium hydride have been used with $NiCl_2$(tmpda) (tmpda = *N*,*N*,*N*′,*N*′-tetramethyl-1,3-propanediamine) to deposit intermetallic Ni_3Sn_2 and Ni_2Ge films at 160 °C and 180 °C, respectively.[18,19] While the processes did not result in Ni metal, the studies clearly indicated that these hydrides do have reducing capabilities. In addition, they attract interest in the applicability of nickel halide precursors in ALD. The advantages of the halide precursors are their simplicity, availability, low price and good reactivity with many co-precursors. Their disadvantages might be limited volatility, the corrosiveness of the byproducts, and possible halide contamination in the deposited films.

1,4-Bis(trimethylsilyl)-1,4-dihydropyrazine ($(Me_3Si)_2DHP$) and 1,4-bis(trimethyl)-2-methyl-2,5-cyclohexadiene ($(Me_3Si)_2CHD$) are intriguing reducing agents which have been used together with $TiCl_4$ and $SnCl_4$ to deposit titanium and tin films, respectively.[20,21] Titanium especially has a low standard redox potential of $E^\circ = -1.63$ V, indicating that $(Me_3Si)_2DHP$ is a powerful reducing agent. While the previous studies[20–22] have shown that $(Me_3Si)_2DHP$ and $(Me_3Si)_2CHD$ are good reducing agents, they have been demonstrated to work with only metal chlorides, which is understandable because in the reactions of these compounds with metal chlorides a highly favorable byproduct of trimethylchlorosilane is formed. However, as shown in this study, $(Me_3Si)_2DHP$ does not afford good nickel films from the adducts of nickel halides.

In this work 1,4-bis(trimethylgermyl)-1.4-dihydropyrazine ($(Me_3Ge)_2DHP$) (Fig. 1) is introduced as a considerably more reactive reducing agent than $(Me_3Si)_2DHP$. $(Me_3Ge)_2DHP$ is used together with dichlorobis(triethylphosphine)nickel(II) ($NiCl_2(PEt_3)_2$) (Fig. 1) for the ALD of nickel metal films at a low temperature of 110 °C. Both precursors are new to ALD. $NiCl_2(PEt_3)_2$ is one compound in a series of phosphine adducts of nickel halides studied along with the cobalt counterparts. The findings of these phosphine adducts are also presented in this work. The phosphine adducts are a continuation of the series of amine adducts of nickel and cobalt halides[18,19,23,24] that we have been studying as possible ALD precursors. Among the phosphine adducts, $NiCl_2(PEt_3)_2$ was identified as one viable candidate with sufficient thermal stability and good volatility, achieving low-temperature ALD.

Experimental section

Precursor synthesis and characterization

Synthesis and all manipulation of the compounds were performed under rigorous exclusion of air and moisture using Schlenk techniques and an argon-filled glove box. Me_3GeCl (Gelest), Li granules (Aldrich), pyrazine (Aldrich, >99%), anhydrous $NiCl_2$ (for synthesis, Aldrich), anhydrous $CoCl_2$ (99+%, Strem) and PEt_3 10 wt% in hexane (ABCR, 99%) were used as received. Tetrahydrofuran (THF) was distilled freshly from the sodium benzophenone ketyl radical and sodium metal.

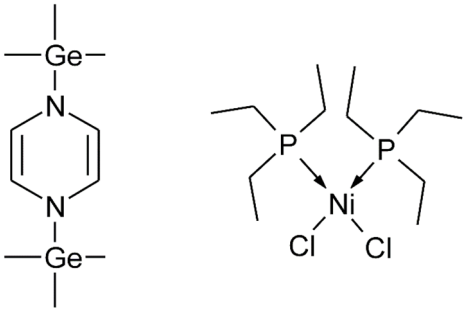

Fig. 1 Structures of $(Me_3Ge)_2DHP$ and $NiCl_2(PEt_3)_2$.

Thermogravimetric analysis (TGA) was performed using Mettler Toledo TGA/DSC 3+ equipment. Measurements were performed under a flowing 1 atm N_2 atmosphere and the 10–11 mg samples were heated from 25 to 600 °C at a rate of 10 °C min^{-1}. Melting points were determined from the SDTA data measured using TGA/DSC 3+ equipment. NMR spectra were measured using a Bruker Avance 400 MHz spectrometer. ^1H and ^{13}C shifts are referenced to internal solvent resonances and reported in parts per million relative to TMS.

Synthesis of 1,4-bis(trimethylgermyl)-1,4-dihydropyrazine. 0.525 g (75.6 mmol) of lithium granules was weighed into a 600 ml Schlenk bottle. 250 ml of THF was added. The reaction vessel was cooled to −15 °C. Magnetic stirring was applied. 5.000 g (32.6 mmol) of Me_3GeCl and 1.300 g (16.2 mmol) of pyrazine dissolved in 100 ml of THF were added to this mixture through a dropping funnel in 3 hours. The solution was left to stir overnight at −15 °C. The unreacted lithium was filtered off with a Schlenk sinter. The filtrate was evaporated to dryness. The resulting yellow-orange solid (5.380 g) was transferred into the sublimation apparatus and sublimed at 80–100 °C/0.05 mbar. Yield 4.430 g (86.7%), orange solid. M.p. 52–79 °C. ^1H NMR (benzene-d_6, 400.14 MHz, 25 °C): δ = 0.16 (s, 18 H, Me), 4.71 (s, 4 H, =CH–N) ppm. ^{13}C NMR (benzene-d_6, 100.61 MHz, 25 °C): δ = −1.57 (s, Ge(CH_3)), 119.20 (s, =CH–N) ppm.

Synthesis of $NiCl_2(PEt_3)_2$. 5.00 g (38.58 mmol) of anhydrous $NiCl_2$ was weighed into a 300 ml Schlenk bottle. 150 ml of THF was added. To this solution, 9.12 g (77.18 mmol) PEt_3 was added with a syringe. The reaction mixture was refluxed for 4 hours and then filtered with a Schlenk sinter in order to remove any undissolved species. The resulting dark brown solution was evaporated to dryness. Yield: 12.64 g (89.5%), red-brown solid, m.p. 109–113 °C. Sublimes at 80–120 °C/0.3 mbar (98% yield). ^1H NMR ($CDCl_3$, 400.14 MHz, 25 °C): δ = 1.31 (t, 18 H, Me), 1.76 (q, 12 H, PCH_2) ppm. ^{13}C NMR ($CDCl_3$, 100.61 MHz, 25 °C): δ = 8.38 (s, CH_3), 13.38 (s, PCH_2) ppm.

A similar synthesis procedure was used for all other phosphine adducts of nickel halides.

Synthesis of $NiBr_2(PEt_3)_2$. 0.70 g (3.20 mmol) of anhydrous $NiBr_2$ and 0.756 g (6.40 mmol) of PEt_3 were used. Yield: 1.43 g (98.5%), violet-brown solid, m.p. 105–109 °C. Sublimes at 100–130 °C/0.3 mbar (98% yield). ^1H NMR ($CDCl_3$, 400.14 MHz, 25 °C): δ = 1.30 (br, 18 H, Me), 2.13 (br, 12 H, PCH_2) ppm. ^{13}C NMR ($CDCl_3$, 100.61 MHz, 25 °C): δ = 9.19 (s, CH_3), 16.34 (s, PCH_2) ppm.

Synthesis of $NiI_2(PEt_3)_2$. 0.28 g (0.90 mmol) of anhydrous NiI_2 and 0.22 g (1.86 mmol) of PEt_3 were used. Yield: 0.44 g (88.0%), brown solid, m.p. 88–92 °C. Sublimes at 80–120 °C/0.3 mbar (98% yield). ^1H NMR ($CDCl_3$, 400.14 MHz, 25 °C): δ = 1.28 (t, 18 H, Me), 2.78 (q, 12 H, PCH_2) ppm. ^{13}C NMR ($CDCl_3$, 100.61 MHz, 25 °C): δ = 10.37 (s, CH_3), 22.03 (s, PCH_2) ppm.

Synthesis of $NiCl_2(PMe_3)_2$. 0.46 g (3.55 mmol) of anhydrous $NiCl_2$ and 0.540 g (7.10 mmol) of PMe_3 were used. Yield: 0.90 g (90.0%), brown solid, m.p. 202–206 °C. Sublimes at 70–90 °C/0.3 mbar (98% yield). ^1H NMR ($CDCl_3$, 400.14 MHz, 25 °C): δ = 1.27 (s, 18 H, Me) ppm. ^{13}C NMR ($CDCl_3$, 100.61 MHz, 25 °C): δ = 12.22 (s, CH_3) ppm.

Synthesis of $NiBr_2(PMe_3)_2$. 0.59 g (2.70 mmol) of anhydrous $NiBr_2$ and 0.41 g (5.40 mmol) of PMe_3 were used. Yield: 0.97 g (97.0%), violet-brown solid, m.p. 184–188 °C. Sublimes at 80–100 °C/0.3 mbar (95% yield). ^1H NMR ($CDCl_3$, 400.14 MHz, 25 °C): δ = 1.58 (s, 18 H, Me), 1.68 (q, 12 H, PCH_2) ppm. ^{13}C NMR ($CDCl_3$, 100.61 MHz, 25 °C): δ = 15.12 (s, CH_3) ppm.

Synthesis of $NiI_2(PMe_3)_2$. 0.34 g (1.09 mmol) of anhydrous NiI_2 and 0.17 g (2.23 mmol) of PMe_3 were used. Yield: 0.45 g (90.0%), violet-black solid, m.p. not observed. Sublimes at 70–120 °C/0.3 mbar (92% yield). ^1H NMR ($CDCl_3$, 400.14 MHz, 25 °C): δ = 0.62 (br, 18 H, Me) ppm.

Synthesis of $CoCl_2(PEt_3)_2$. 0.20 g (1.54 mmol) of anhydrous $CoCl_2$ was weighed into a 100 ml Schlenk bottle. 30 ml of CH_2Cl_2 was added. To this solution 0.36 g (3.08 mmol) of PEt_3 was added with a syringe. In 15 min, all solid $CoCl_2$ was dissolved. After 1 hour the solvent was removed under vacuum and in a warm water bath. Light blue solid, m.p. 99–105 °C. An attempt at sublimation at 90–130 °C/0.3 mbar resulted in partial decomposition or loss of the PEt_3 ligands and the sublimation yield after 20 hours was only 28%.

A similar synthesis procedure was used for all other phosphine adducts of cobalt halides.

Synthesis of $CoBr_2(PEt_3)_2$. 2.00 g (9.14 mmol) of anhydrous $CoBr_2$ and 2.16 g (18.28 mmol) of PEt_3 were used. Light blue solid, m.p. 128–135 °C. Sublimation at 140 °C/0.3 mbar resulted in 91.5% yield.

Synthesis of $CoI_2(PEt_3)_2$. 0.57 g (1.82 mmol) of anhydrous CoI_2 and 0.43 g (3.64 mmol) of PEt_3 were used. Light green solid, m.p. 123–130 °C. Sublimation at 140 °C/0.3 mbar resulted in 90% yield.

Synthesis of $CoCl_2(PMe_3)_2$. 0.46 g (3.54 mmol) of anhydrous $CoCl_2$ and 0.54 g (7.09 mmol) of PMe_3 were used. Dark green solid, m.p. 111–117 °C. Sublimation at 140 °C/0.3 mbar resulted in <2% yield.

Synthesis of $CoBr_2(PMe_3)_2$. 0.59 g (2.70 mmol) of anhydrous $CoBr_2$ and 0.42 g (5.52 mmol) of PMe_3 were used. Green-blue solid, m.p. 128–132 °C. Sublimation at 110–140 °C/0.3 mbar resulted in 47% yield.

Synthesis of $CoI_2(PMe_3)_2$. 0.34 g (1.09 mmol) of anhydrous CoI_2 and 0.17 g (2.23 mmol) of PMe_3 were used. Black-violet solid, m.p. 139–146 °C. Sublimation at 120–140 °C/0.3 mbar resulted in 81% yield.

Film deposition

Deposition experiments were performed in an F-120 hot-wall flow-type ALD reactor (ASM Microchemistry). The reactor had a pressure of approximately 10 mbar and N_2 (AGA 5.0) was used as the carrier and purging gas. Both $NiCl_2(PEt_3)_2$ and $(Me_3Ge)_2DHP$ were evaporated from open glass boats held inside the reactor at 100 and 35 °C for $NiCl_2(PEt_3)_2$ and $(Me_3Ge)_2DHP$, respectively. Pulsing was done by inert gas valving and the pulse times were varied from 0.5 to 3.0 s. A purge time of 1.0 s was used for most of the depositions. The substrates were 5 × 5 cm^2 native oxide-terminated Si and soda lime glass. In addition, film depositions were tested on Cu, TiN and Al_2O_3 films.

Film characterization

The crystal structure of the films was studied with X-ray diffraction with a PANalytical X'Pert Pro MPD X-ray diffractometer. A grazing incidence geometry was used with Cu Kα (λ = 1.54 Å) radiation having an incidence angle of 1°. The results were analysed with the PANalytical Highscore Plus 4.1 software. Diffractograms were analysed with the MAUD 2.992 software to determine the size of the crystallites.[25]

Film thicknesses were measured with energy-dispersive X-ray spectrometry (EDS) using an Oxford INCA 350 connected to a Hitachi scanning electron microscope (SEM). An electron voltage of 20 kV was used and the thickness was calculated from Ni Kα X-ray lines with the GMRFILM program using a bulk density of 8.9 g cm^{-3} for nickel.[26] An uncertainty of 5% was estimated for the thickness measurements due to a slight fluctuation of the electron beam current and possible deviations from the bulk density. The film composition was measured by time-of-flight elastic recoil detection analysis (ToF-ERDA) using a 40 MeV $^{127}I^{7+}$ ion beam.

A field emission scanning electron microscope (FESEM) was used to evaluate the morphology and nucleation of the films. Sheet resistances were measured from the films deposited on soda lime glass substrates using a four-point probe (CPS Probe Station, Cascade Microtech combined with a Keithley 2400 SourceMeter). Sheet resistance was measured as an average from nine measurement points uniformly distributed across the film/substrate. The resistivity was obtained by multiplying the sheet resistance by the film thickness.

Atomic force microscopy (AFM, Veeco Multimode V instrument) was used to study the surface morphology and roughness of the films. A Si probe with a nominal tip radius of 10 nm and a spring constant of 3 N m^{-1} was used to capture images in air from the films deposited on the Si substrates. Roughness was calculated as a root-mean-square value (R_q) from the flattened images. Flattening was performed to remove artefacts from the sample tilt and scanner bow.

Further characterization was performed with XPS and Raman spectroscopy. The XPS measurements were performed with a Prevac system EA-15 hemispherical electrostatic energy analyser and RMC50 monochromatic X-ray source with an Al Kα anode (1486.7 eV) operated at 220 W. The base pressure during all measurements was 10^{-10} mbar. The pass energy for the measurements was 50 eV and that of the slit was C 0.3 × 25. Prior to the measurements the films were rastered for 1 hour with 1 keV He^+ ions over an area of 5 mm × 2 mm to remove oxygen and other impurities from the surface of the films. The peak fitting was achieved with CasaXPS by GL line shape. Raman spectroscopy studies were conducted with a confocal Raman microscope (NT-MDT Ntegra) with a 532 nm laser and a 100× objective. Micro-Raman spectra were measured in the backscattering geometry. The nominal output power of the laser was 20 mW. During each measurement 20 exposures with 4.0 s exposure time were used. Nickel foil (0.5 mm thick, annealed, 99.5%, Alfa Aesar) was used for a reference measurement.

Results and discussion

Metal precursors

Earlier we introduced diamine adducts of nickel and cobalt halides as cost-effective precursors to ALD.[18,19,23,24] Nickel and cobalt halides as such are solids with polymeric structures and poor volatility. Sublimation temperatures above 350 °C are typically needed. Adding appropriate amines into the halides gives thermally stable monomeric adducts with dramatically enhanced volatility. $NiCl_2$(tmpda) sublimes cleanly at 160–180 °C/0.5 mbar and withstands temperatures up to 250 °C.[24] As compared with other known Ni and Co precursors, this volatility is among the average values. However, especially when elemental metal films are to be deposited, the volatility should be as high as possible to reach the lowest possible deposition temperature to minimize the agglomeration for achieving smoother films, and thereby continuous films at lower thickness.

We have now studied the phosphine adducts of the nickel and cobalt halides. Initially a bidentate diphosphine ligand bis(diethylphosphino)ethane was studied as the adduct ligand. It was found that these compounds are thermally quite stable (>320 °C) but their volatilities are low (vacuum sublimation required temperatures over 240 °C). Surprisingly, the adducts with two monodentate alkylphosphines, PMe_3 and PEt_3, behave quite differently. The monodentate alkylphosphine adducts of nickel halides have very high volatility so that the compounds can be sublimed well at 70–130 °C/0.3 mbar. Unfortunately, the thermal stability of the adducts is also low so that, *e.g.* the upper limit for the ALD with $NiCl_2(PEt_3)_2$ is as low as 130 °C. In the case of cobalt, the thermal stability is similar or higher but the volatility is also lower so that temperatures above 120 °C are needed for vacuum sublimation. Because of the small window between the evaporation temperature and the onset temperature for thermal decomposition, the ALD of cobalt was found to be impossible even though some of the adducts, especially those of $CoBr_2$ and CoI_2, can be sublimed with over 90% yields.

It seems to be a general trend that among the adducts of the different halides of cobalt and nickel the thermal stability increases in the order chloride < bromide < iodide. The trend seems to be more pronounced with cobalt. This observation is likely due to the decreasing electron affinity in the halide series that makes the metal a better π back donor, which in turn causes the phosphine ligands to bond more strongly to the metal. The bonding strengths of the phosphines may also be explained by the Lewis hard–soft acid–base (HSAB) symbiotic effect; when softer anionic ligands (here Br and I) are bonded to the metal ion, they soften the metal acidity and thereby make bonding with soft bases like phosphines more favorable.

Despite the substantially increasing molecular weight from the chlorides to the iodides, the volatilities of the compounds remain quite similar – only a slight decrease is observed upon going from the chlorides to the iodides. When comparing the two phosphine ligands, PMe_3 and PEt_3, the adducts with the

PMe_3 ligand have better volatility but also lower thermal stability. However, overall, the differences seem to be quite small.

The TG curves measured under a 1 atm flowing nitrogen atmosphere for the abovementioned $NiX_2(PR_3)_2$ (R = Me, Et) adducts are shown in Fig. 2. The measurements show large residues and it is likely that the weight losses are mostly due to thermal decomposition. However, the residual masses at 400 °C, *i.e.* after the first step of the weight loss (15–31%), are much lower than the nickel halide contents of the compounds (35–67%) and therefore it is not only the phosphine ligands that are evaporated. Part of the complex may evaporate intact or decomposition other than simple loss of the phosphine ligands might take place. The PMe_3 adducts show weight loss at a lower temperature and, despite the larger metal content, they leave smaller residues than the PEt_3 adducts, with $NiCl_2(PMe_3)_2$ being an exception with a residue similar to $NiCl_2(PEt_3)_2$. $NiBr_2(PMe_3)_2$ and $NiI_2(PMe_3)_2$ both show residues of 15% while the $NiBr_2$ and NiI_2 contents are 59 and 67%, respectively. This might be interpreted to indicate better volatility. However, because both decomposition and evaporation are taking place in the TGA performed at 1 atm and with uncertainty regarding what really happens to the compounds during heating, the sublimation temperatures and yields from vacuum sublimation experiments give generally a better view of the volatility of the compounds. If the weight losses are considered to be mostly due to the decomposition, the PEt_3 adducts seem to be thermally more stable than the PMe_3 adducts, and among the halides the adducts of nickel iodides are more stable than those of nickel chlorides and bromides. In the vacuum sublimation experiments it was seen that the PMe_3 adducts do start to sublime at lower temperatures than the PEt_3 adducts (70 *vs.* 80 °C) and also sublime faster. The sublimation yields were 92–98%.

The TG curves measured for the $CoX_2(PR_3)_2$ (R = Me, Et) compounds (Fig. S1†) mainly show decomposition. For the phosphine adducts of $CoCl_2$ the residual masses after the first mass loss step (46 and 35% for the PMe_3 and PEt_3 adducts, respectively) are exactly the theoretical amounts of $CoCl_2$ (46 and 35%) in the compounds, indicating the loss of the phosphine ligands. For the bromides and iodides, the decomposition seems to be a more complicated process. However, at least in the case of the PEt_3 adducts the onset of the weight loss is seen at a much higher temperature with the bromides and iodides than with the chlorides, indicating better thermal stability rather than lower volatility.

In the light of these thermal property studies, it is difficult to conclude which of the nickel precursors will show the best performance in actual ALD usage. Out of the phosphine adducts of nickel halides the PMe_3 adducts have the best volatility and among these $NiI_2(PMe_3)_2$ might be the most thermally stable one. The PEt_3 adducts are slightly less volatile than the PMe_3 adducts but the thermal stability seems to be higher. In this work, ALD studies were conducted using $NiCl_2(PEt_3)_2$, which has average properties among the adducts synthesized. The selection was further affected by the above reasoning that because of the favorable byproduct the metal chloride might be more reactive with $(Me_3Si)_2DHP$ than the bromide and iodide. The chloride ion is also smaller in size and together these properties might lead to higher growth rates.

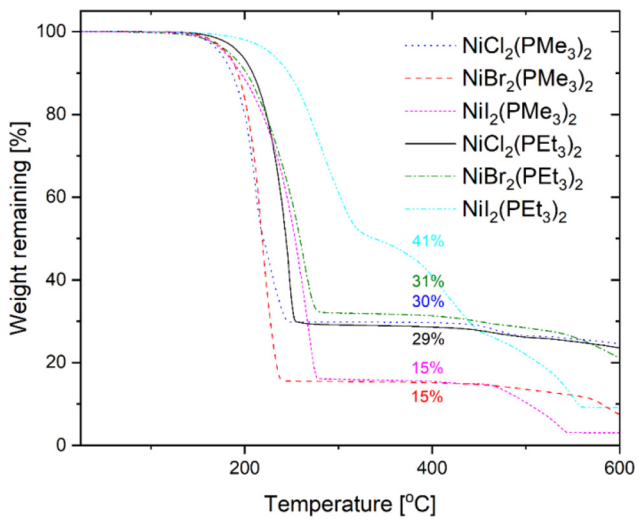

Fig. 2 TG curves measured for different $NiX_2(PR_3)_2$ (X = Cl, Br, I; R = Me, Et) compounds.

Reducing agent

Klesko *et al.*[20] and Stevens *et al.*[21] showed that $(Me_3Si)_2DHP$ and $(Me_3Si)_2CHD$ are good reducing agents for metal halides. $(Me_3Si)_2DHP$ is hypothesized to react with metal halides, forming trimethylsilylhalide and a pyrazinediyl metal compound, which immediately rearranges so that the metal cation is reduced and the anti-aromatic dihydropyrazine dianion is oxidized to aromatic pyrazine.[27] However, our ALD experiments indicated that $(Me_3Si)_2DHP$ does not afford good nickel films from $NiCl_2(PEt_3)_2$. The growth rate was low and only nanoparticles were deposited after 1000 cycles at 110 °C (Fig. 3). Because of the unsatisfactory result, a more reactive reducing agent was still desired. Thus, a trimethylgermyl analogue of $(Me_3Si)_2DHP$, $(Me_3Ge)_2DHP$, was synthesized. $(Me_3Ge)_2DHP$ is expected to react similarly to $(Me_3Si)_2DHP$.

Using exactly the same synthesis procedure as that used for the trimethylsilyl analogue, the synthesis yields were low (0–20%). By optimizing the synthesis the yield was increased to 87%. $(Me_3Ge)_2DHP$ is an extremely air- and moisture-sensitive orange solid that melts at 52–79 °C and can be sublimed cleanly at 80–100 °C/0.3 mbar. According to the ALD experiments, the compound seems to be stable up to only 200 °C, which is lower than the value for the trimethylsilyl analogue that can be used at least up to 240 °C (ref. 20) but probably also at much higher temperatures. This is likely due to the clearly weaker N–Ge bond compared with the N–Si bond. The bonding energies have been estimated to be around 324 and 256 kJ mol^{-1}, for N–Si and N–Ge, respectively.[28] However, apparently for the same reason for the weaker N–Ge bond, $(Me_3Ge)_2DHP$ also seems to be more reactive than

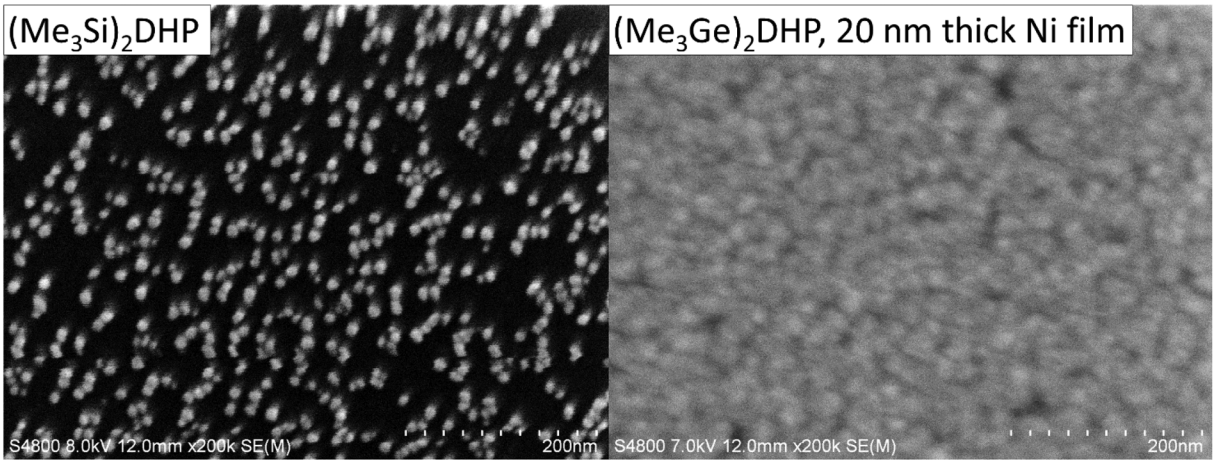

Fig. 3 Films deposited at 110 °C from $NiCl_2(PEt_3)_2$ and either $(Me_3Si)_2DHP$ or $(Me_3Ge)_2DHP$. (With $(Me_3Si)_2DHP$ only a layer of Ni islands was deposited, indicating a much lower growth rate at the same temperature.)

$(Me_3Si)_2DHP$. Considering simply the bond energies, the reaction where the Ge–N bond (256 kJ mol^{-1}) is broken and Ge–Cl (373 kJ mol^{-1}) is formed is more favourable than the reaction where Si–N (324 kJ mol^{-1}) is broken and Si–Cl (416 kJ mol^{-1}) is formed, *i.e.* the reaction enthalpy is more negative for $(Me_3Ge)_2DHP$. Thus it seems that what is lost in the thermal stability is gained in the reactivity. Fortunately, in this case, the thermal stability is sufficient for low-temperature processes

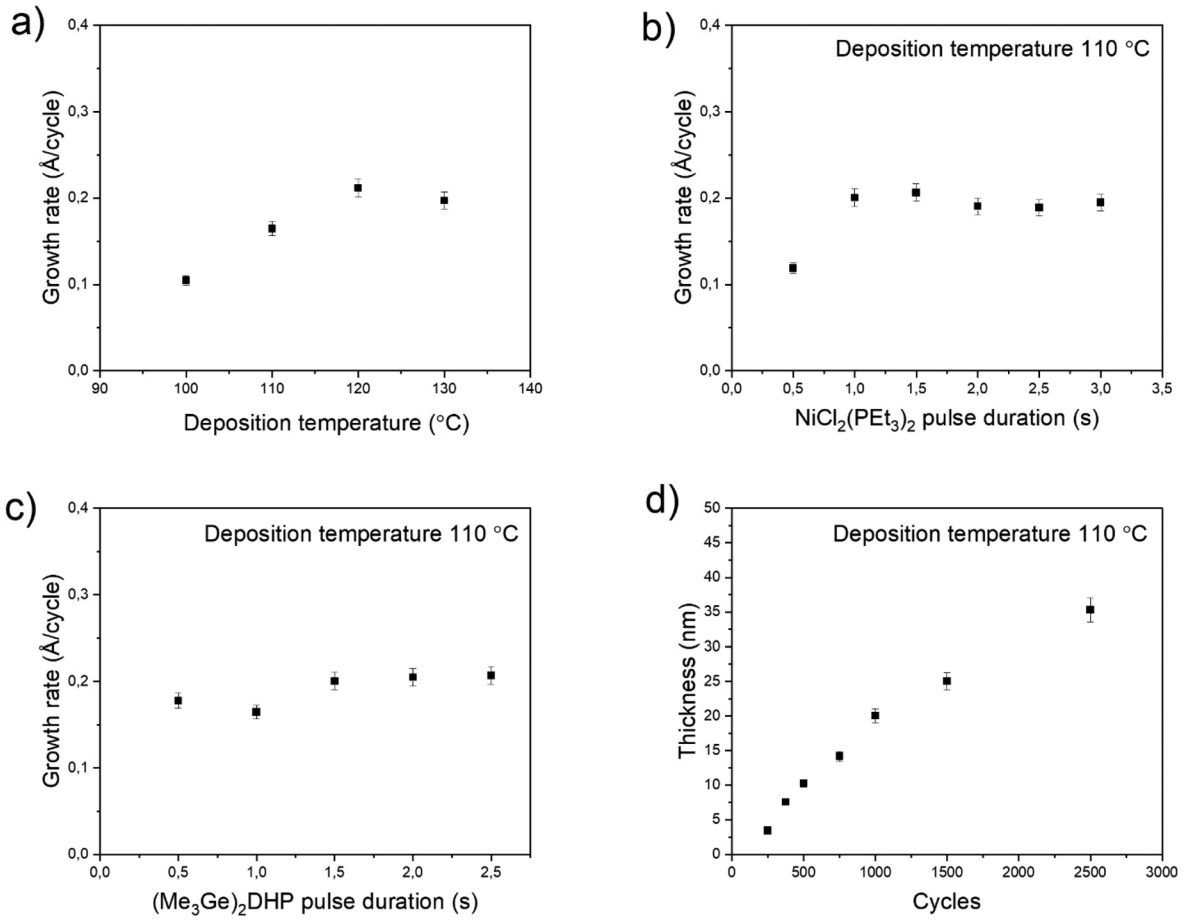

Fig. 4 Growth characteristics of the $(Me_3Ge)_2DHP$ + $NiCl_2(PEt_3)_2$ process. The growth rate as a function of the deposition temperature (a), $NiCl_2(PEt_3)_2$ pulse length (b), and $(Me_3Ge)_2DHP$ pulse length (c). Film thickness as a function of number of cycles (d).

that are also otherwise desired. In general, it appears that the weak N–Ge bond makes $(Me_3Ge)_2DHP$ a potentially more generic reducing agent than $(Me_3Si)_2DHP$.

Nickel film deposition and growth characteristics

To evaluate $(Me_3Ge)_2DHP$ as a more reactive reducing agent, it was tested with $NiCl_2(PEt_3)_2$. A fully continuous, smooth and uniform Ni film was deposited at 110 °C, indicating a much higher reactivity and growth rate (Fig. 3). While $(Me_3Ge)_2DHP$ and $(Me_3Si)_2DHP$ are structurally similar molecules, it is clear that their reactivities are very different. Thus, this study focuses on Ni ALD from $NiCl_2(PEt_3)_2$ and $(Me_3Ge)_2DHP$.

The growth characteristics of the $NiCl_2(PEt_3)_2$–$(Me_3Ge)_2DHP$ process are presented in Fig. 4. The growth rate was investigated as a function of temperature ranging from 100 to 130 °C. The lower limit was dictated by using the sublimation temperature of the nickel precursor (T_{sub} = 100 °C). At 130 °C, the nickel precursor seemed to decompose extensively, as indicated by the formation of $NiCl_2$ at the hot end of the precursor tube. While similar decomposition in the source tube occurred to some degree also at 120 and 110 °C, no effect on the film growth was observed and saturation of the growth rate could be achieved at 110 °C. The growth rate was found to be temperature dependent, first increasing with temperature and then remaining at the level of 0.2 Å per cycle (Fig. 4a). The resistivity of the films likewise increased with temperature from 30 to 50 μΩ cm, most likely due to the increased impurity content caused by the slight decomposition of $NiCl_2(PEt_3)_2$. 110 °C was chosen as the optimal deposition temperature as the best alternative for the resistivity and growth rate.

Saturation tests were performed with both precursors at 110 °C (Fig. 4b and c). These depositions were performed with 1000 cycles and 1.0 s purges. Saturation of the growth rate to 0.2 Å per cycle was observed with both precursors. With $NiCl_2(PEt_3)_2$ the saturation was reached with a 1.0 s pulse time and with $(Me_3Ge)_2DHP$ it was achieved with a 1.5 s pulse time.

In a typical ALD process, the film thickness increases linearly with cycle number. However, here two regimes in the growth rate could be observed (Fig. 4d). Up to 20 nm, the growth rate was a constant 0.2 Å per cycle, but then it decreased to 0.1 Å per cycle. As the growth rate change occurs at about the same time when the film becomes fully continuous (1000 cycles, 20 nm, see below), the decrease in the growth rate can be attributed to a decreasing surface area. A smaller surface area means less adsorption sites for the metal precursor and thus less film is deposited in each cycle. This is a quite common observation in the ALD of metals.[29] The sufficiency of the 1.0 s purge time was confirmed by doubling it to 2.0 s without any effect on the growth rate. The films had good uniformity across the substrate (Fig. S2†). The films were deposited successfully also on the TiN, Al_2O_3 and Cu films without any significant change in the growth rate. The equal

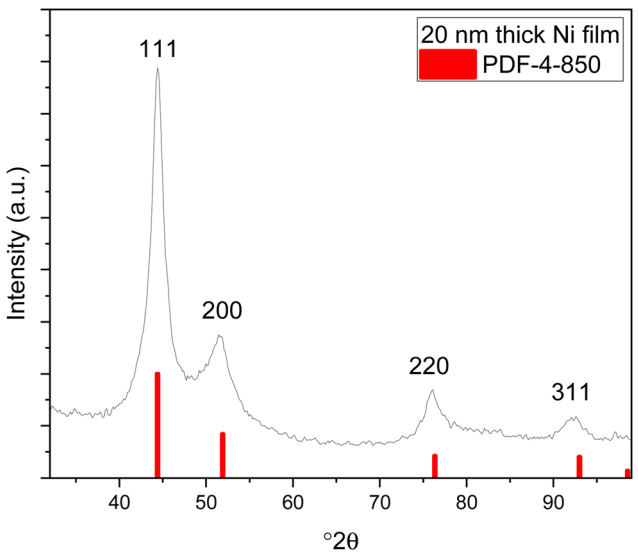

Fig. 5 Grazing incidence X-ray diffractogram of the 20 nm Ni film deposited at 110 °C.

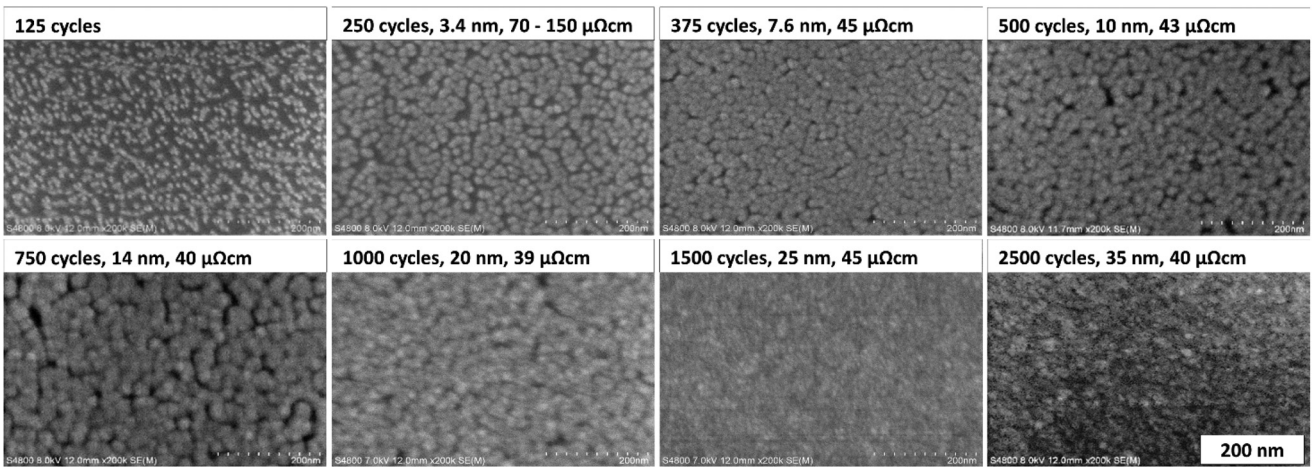

Fig. 6 SEM images of Ni films deposited at 110 °C with varying number of cycles with their respective thicknesses and resistivities.

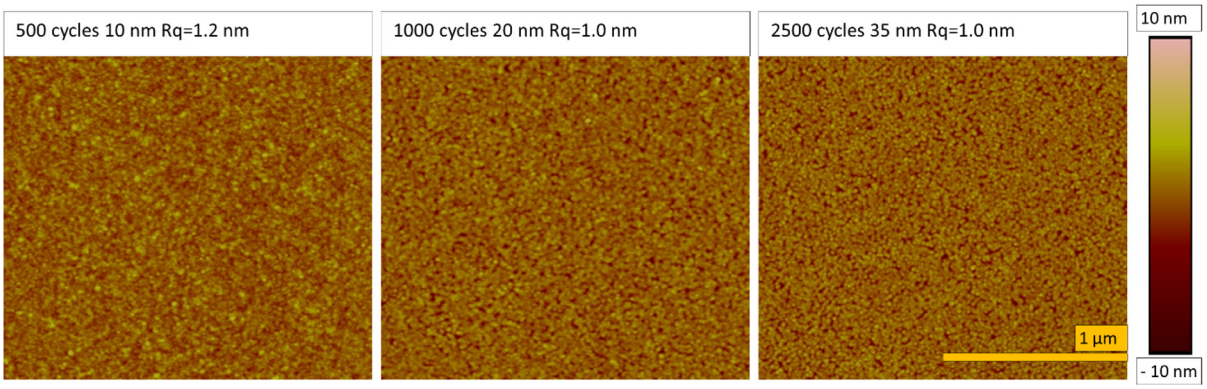

Fig. 7 AFM images taken of the Ni films deposited at 110 °C with varying number of cycles.

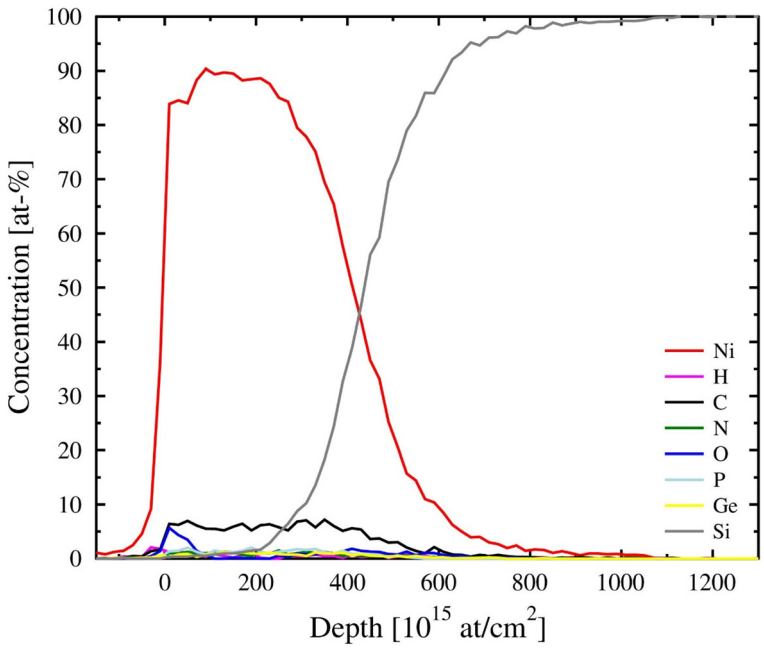

Fig. 8 ToF-ERDA elemental depth profiles of 35 nm thick Ni film deposited at 110 °C.

growth on the insulators and metals indicates that the process is not sensitive to the underlying material.

Film characterization

XRD measurements were conducted with the films deposited on silicon at different temperatures, and with the films deposited under optimal conditions (at 110 °C with saturative pulses) with different thicknesses (20 nm and 35 nm). All the films exhibited similar X-ray diffractograms with reflections matching those of fcc nickel (Fig. 5, ICDD PDF file 4-850). The large width of the reflections indicates small crystallites. Fitting of the diffractograms indicated that the crystallite sizes were below 10 nm, but the background shape under the peaks indicates that even smaller crystallites are present in the film.

The morphology and nucleation of the films were studied with SEM and AFM. The films were smooth and became pinhole free when the thickness exceeded 20 nm (Fig. 6). The grain size was small with a lateral size of approximately 20–30 nm and this is also demonstrated by wide reflections in

Table 1 Elemental composition of the 35 nm thick Ni film deposited at 110 °C

Element	At%
Ni	86.8 ± 0.5
C	7.03 ± 0.16
O	1.46 ± 0.07
P	1.39 ± 0.07
Ge	1.03 ± 0.05
H	0.93 ± 0.08
N	1.14 ± 0.06
Cl	<0.2

XRD (Fig. 5). The root mean square roughness (R_q) of the films was approximately 1.2 nm at 10 nm thickness and slightly decreased to 1.0 nm after the film thickness exceeded 20 nm and the films became fully continuous (Fig. 7). The R_q values are the average from three different measurements. For metals, the films are very smooth, which is typical also of other published ALD Ni films with roughness values varying between 0.5 and 1.5 nm.[12,15,17]

Elemental composition of the films was studied with ToF-ERDA measurements (Fig. 8 and Table 1). The films were

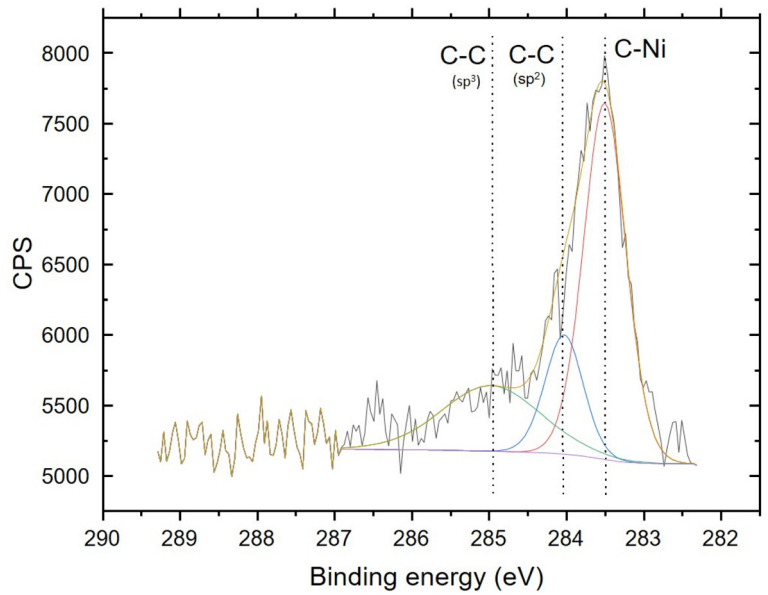

Fig. 9 The C 1s XPS spectrum of the 35 nm thick Ni film deposited at 110 °C. The fitted peaks correspond to the different types of carbon bonds and the clearly dominant peak is attributed to the C–Ni bond.

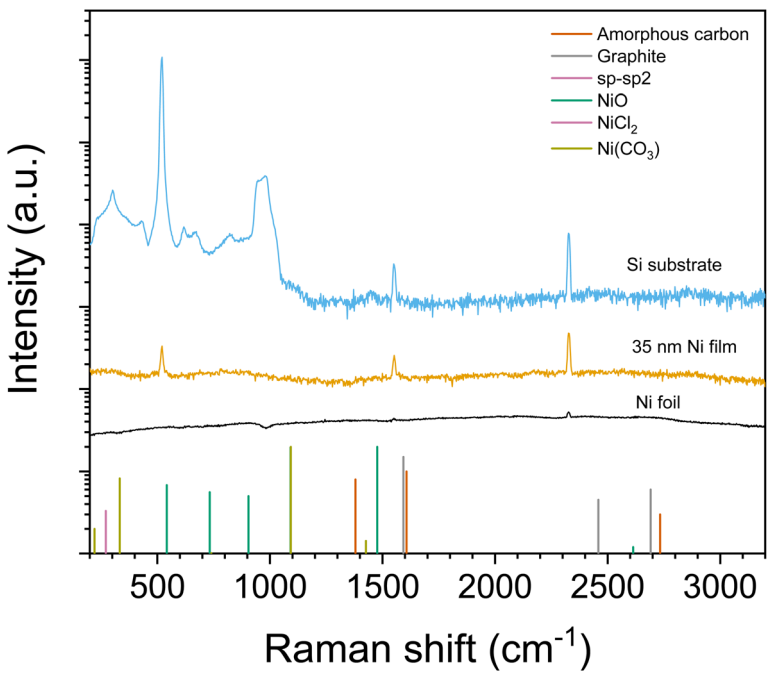

Fig. 10 Raman spectra from a 35 nm Ni film deposited at 110 °C and, for reference, from a nickel metal foil and the Si substrate. Band positions for selected phases are shown with bars. Carbon and $NiCl_2$ band positions are from Wu *et al.*[32] and Lockwood *et al.*[34] respectively. NiO and $Ni(CO_3)$ band positions are determined from ROD 3500021 and RRUFF R040157 entries respectively.

mostly metallic nickel with about 7 at% of carbon. The other impurities are at levels below 1.5 at%. The very low chlorine content is notable and indicates efficient reduction by $(Me_3Ge)_2DHP$. Oxygen is found only from the surface of the film, which refers to post-deposition oxidation in air. Because the hydrogen content is also below 1 at%, a major part of the carbon detected must be in other forms than hydrocarbon residues.

The chemical character of the 7 at% carbon detected in the films was studied using XPS. The chemical state of the carbon was revealed to be mostly carbidic (Fig. 9). The spectrum is almost identical to the one presented by Furlan *et al.*[30] for a nickel film with 5 at% carbon. Besides the carbon and oxygen from the surface, no impurities could be reliably detected with XPS.

The chemical character of the carbon was studied further using Raman spectroscopy. Similar to all metals with the monoatomic lattice (fcc and bcc metals), metallic nickel does not show Raman bands. In contrast, carbon impurities show active Raman bands that should be seen if they are present. These include graphite, graphene, amorphous carbon and highly disordered carbon.[31–33] Since none of the bands were detected (Fig. 10), the carbon in the films must be carbidic in nature and concealed within the fcc crystal structure, invisible in the Raman spectra. As a further proof of all the other forms of carbon besides Ni_3C being easily detectable with Raman, Raman measurements from Co films that had similar amounts of carbon did show peaks of amorphous carbon (not shown). This indicates that this amount of carbon could clearly be seen with Raman if not carbidic.

The resistivities of the films were measured from soda lime glass substrates with the four-point probe. The films exhibited a resistivity of approximately 40 μΩ cm once they had become fully continuous. Nickel has a bulk resistivity of 7 μΩ cm.[35] It is common for thin films to have higher resistivity than bulk materials, and the incorporated carbon is also known to increase the resistivity. Furlan *et al.*[30] studied the resistivity of the magnetron-sputtered $Ni_{1-x}C_x$ films. A carbon content of 3 at% resulted in a resistivity of 30 μΩ cm. Increasing the carbon content to 5 at% increased the resistivity to 62 μΩ cm. The resistivity increased linearly up to 16.3 at% of carbon, which was exceeded and the films turned from polycrystalline to amorphous, which caused a major increase in the resistivity. The resistivity values reported for the ALD-deposited Ni films range between 19 and 27 μΩ cm while the carbon content is less than 5 at%.[12,15,17] Our results are in line with these, as increasing carbon content increases the resistivity and our films contain slightly more carbon than the other ALD Ni films. Furthermore, our Ni films have small grain sizes, which is also a factor increasing their resistivity.

Conclusions

A new low-temperature reducing agent, $(Me_3Ge)_2DHP$, was synthesized and found to be more efficient than the known $(Me_3Si)_2DHP$. Similar to $(Me_3Si)_2DHP$, $(Me_3Ge)_2DHP$ is expected to be an efficient reducing agent for metal halides. A number of phosphine adducts of nickel and cobalt halides were studied as possible precursors for ALD. It was found that nickel halides with simple monodentate phosphines PEt_3 and PMe_3 have exceptionally good volatility among the adducts of nickel halides. Their thermal stability is sufficient and allows ALD usage.

$NiCl_2(PEt_3)_2$ was combined with $(Me_3Ge)_2DHP$ to deposit metallic nickel films at a low temperature of 110 °C. This is the lowest reported deposition temperature for Ni ALD to date. The films exhibited similar resistivity to nickel films deposited earlier with ALD and while they had a small amount of carbon, it was in carbidic form and thus less detrimental to the properties of the films than amorphous carbon or graphite would be expected to be. The combination of high quality films and a low deposition temperature show potential for multiple applications. Furthermore, both precursors are novel precursors and especially $(Me_3Ge)_2DHP$ can be combined with other metal halide precursors for opening up new avenues for the ALD of metals at low temperatures.

Conflicts of interest

There are no conflicts to declare.

Acknowledgements

Mikko Heikkilä is acknowledged for the valuable help with the XRD analysis. ASM Microchemistry Oy is gratefully acknowledged for funding this research. The ALD Center Finland is acknowledged for the infrastructure.

References

1 G. Wang, Z. Gao, S. Tang, C. Chen, F. Duan, S. Zhao, S. Lin, Y. Feng, L. Zhou and Y. Qin, *ACS Nano*, 2012, **6**, 11009–11017.
2 T. D. Gould, A. Izar, A. W. Weimer, J. L. Falconer and J. W. Medlin, *ACS Catal.*, 2014, **4**, 2714–2717.
3 J. Zhang, C. Chen, W. Yan, F. Duan, B. Zhang, Z. Gao and Y. Qin, *Catal. Sci. Technol.*, 2016, **6**, 2112–2119.
4 K. Croes, C. Adelmann, C. J. Wilson, H. Zahedmanesh, O. Varela Pedreira, C. Wu, A. Lesniewska, H. Oprins, S. Beyne, I. Ciofi, D. Kocaay, M. Stucchi and Z. Tokei, *Interconnect metals beyond copper: reliability challenges and opportunities*, 2018.
5 D. Choi, *Korean J. Met. Mater.*, 2018, **56**, 605–610.
6 J. A. Kittl, A. Lauwers, O. Chamirian, M. Van Dal, A. Akheyar, M. De Potter, R. Lindsay and K. Maex, *Microelectron. Eng.*, 2003, **70**, 158–165.
7 The future of scalable STT-RAM as a universal embedded memory, **https://www.embedded.com/the-future-of-scalable-stt-ram-as-a-universal-embedded-memory/**.

8 M. Utriainen, M. Kroger-Laukkanen, L. S. Johansson and L. Niinistö, *Appl. Surf. Sci.*, 2000, **157**, 151–158.
9 B. S. Lim, A. Rahtu and R. G. Gordon, *Nat. Mater.*, 2003, **2**, 749–754.
10 K.-W. Do, C.-M. Yang, I.-S. Kang, K.-M. Kim, K.-H. Back, H.-I. Cho, H.-B. Lee, S.-H. Kong, S.-H. Hahm, D.-H. Kwon, J.-H. Lee and J.-H. Lee, *Jpn. J. Appl. Phys., Part 1*, 2006, **45**, 2975–2979.
11 W.-H. Kim, H.-B.-R. Lee, K. Heo, Y. K. Lee, T.-M. Chung, C. G. Kim, S. Hong, J. Heo and H. Kim, *J. Electrochem. Soc.*, 2011, **158**, D1–D5.
12 Y. Zhang, L. Du, X. Liu and Y. Ding, *Nanoscale*, 2019, **11**, 3484–3488.
13 T. J. Knisley, T. C. Ariyasena, T. Sajavaara, M. J. Saly and C. H. Winter, *Chem. Mater.*, 2011, **23**, 4417–4419.
14 J. P. Klesko, M. M. Kerrigan and C. H. Winter, *Chem. Mater.*, 2016, **28**, 700–703.
15 M. M. Kerrigan, J. P. Klesko, K. J. Blakeney and C. H. Winter, *ACS Appl. Mater. Interfaces*, 2018, **10**, 14200–14208.
16 L. C. Kalutarage, P. D. Martin, M. J. Heeg and C. H. Winter, *J. Am. Chem. Soc.*, 2013, **135**, 12588–12591.
17 M. Sarr, N. Bahlawane, D. Arl, M. Dossot, E. McRae and D. Lenoble, *J. Phys. Chem. C*, 2014, **118**, 23385–23392.
18 K. Väyrynen, T. Hatanpää, M. Mattinen, K. Mizohata, K. Meinander, J. Räisänen, J. Link, R. Stern, M. Ritala and M. Leskelä, *Adv. Mater. Interfaces*, 2019, **6**, 1801291.
19 K. Väyrynen, A. Vihervaara, T. Hatanpää, M. Mattinen, M. J. Heikkilä, K. Mizohata, J. Räisänen, M. Ritala and M. Leskelä, *Chem. Mater.*, 2019, **31**, 5314–5319.
20 J. P. Klesko, C. M. Thrush and C. H. Winter, *Chem. Mater.*, 2015, **27**, 4918–4921.
21 E. C. Stevens, M. B. M. Mousa and G. N. Parsons, *J. Vac. Sci. Technol. A*, 2018, **36**, 06A106.
22 C. H. Winter and J. P. Klesko, *US Pat.*, US 20150004315 A1, 2015.
23 K. Väyrynen, T. Hatanpää, M. Mattinen, M. Heikkilä, K. Mizohata, K. Meinander, J. Räisänen, M. Ritala and M. Leskelä, *Chem. Mater.*, 2018, **30**, 3499–3507.
24 K. Väyrynen, T. Hatanpää, M. Mattinen, M. J. Heikkilä, K. Mizohata, J. Räisänen, J. Link, R. Stern, M. Ritala and M. Leskelä, *Phys. Status Solidi A*, 2019, **216**, 1900058.
25 L. Lutterotti, *Nucl. Instrum. Methods Phys. Res., Sect. B*, 2010, **268**, 334–340.
26 R. A. Waldo, *Microbeam Anal.*, 1988, 310–314.
27 T. Saito, H. Nishiyama, H. Tanahashi, K. Kawakita, H. Tsurugi and K. Mashima, *J. Am. Chem. Soc.*, 2014, **136**, 5161–5170.
28 H. Basch, *Inorg. Chim. Acta*, 1996, **252**, 265–279.
29 K. Väyrynen, K. Mizohata, J. Räisänen, D. Peeters, A. Devi, M. Ritala and M. Leskela, *Chem. Mater.*, 2017, **29**, 6502–6510.
30 A. Furlan, J. Lu, L. Hultman, U. Jansson and M. Magnuson, *J. Phys.: Condens. Matter*, 2014, **26**, 415501.
31 B. C. Bayer, D. A. Bosworth, F. B. Michaelis, R. Blume, G. Habler, R. Abart, R. S. Weatherup, P. R. Kidambi, J. J. Baumberg, A. Knop-Gericke, R. Schloegl, C. Baehtz, Z. H. Barber, J. C. Meyer and S. Hofmann, *J. Phys. Chem. C*, 2016, **120**, 22571–22584.
32 J.-B. Wu, M.-L. Lin, X. Cong, H.-N. Liu and P.-H. Tan, *Chem. Soc. Rev.*, 2018, **47**, 1822–1873.
33 A. C. Ferrari, *Solid State Commun.*, 2007, **143**, 47–57.
34 D. J. Lockwood, D. Bertrand, P. Carrara, G. Mischler, D. Billerey and C. Terrier, *J. Phys. C: Solid State Phys.*, 1979, **12**, 3615–3620.
35 J. R. Rumble, *CRC Handbook of Chemistry and Physics*, CRC Press, Taylor & Francis Group, Boca Raton, London, New York, 98th edn, 2017.